Applied Catalysis B: Environmental 180 (2016) 442–450

Contents lists available at ScienceDirect

Applied Catalysis B: Environmental

journal homepage: www.elsevier.com/locate/apcatb

Photocatalytic activity of Fe-modified bismuth titanate pyrochlores: Insights into its stability, photoelectrochemical, and optical responses

William Ragsdale, Satyajit Gupta, Keenan Conard, Steven Delacruz, Vaidyanathan Ravi Subramanian *

Chemical and Materials Engineering Department, University of Nevada, Reno, NV 89557, USA

ARTICLE INFO

Article history:
Received 2 December 2014
Received in revised form 15 April 2015
Accepted 9 June 2015
Available online 23 June 2015

Keywords:
Bismuth titanate
Methyl orange
Photodegradation
Reusability
Photoelectrochemistry

ABSTRACT

This work examines the catalytic activity of a pyrochlore phase bismuth titanate ($Bi_2Ti_2O_7$–BTO) in driving the photo-assisted decomposition of a model pollutant, methyl orange (MO). The photoactivity of the BTO has been probed with the inclusion of Fe with BTO and with the addition of a co-catalyst- Pt external to the Fe-BTO. The addition of Fe enhances BTO photoactivity by ~38%, while the presences of Pt along with Fe demonstrate the most favorable increase at 88% compared to the plain BTO. The MO degradation follows a pseudo first order kinetics. Under 100% visible light illumination, all catalysts demonstrate photoactivity. Specifically, a 10%, 15%, and 21% degradation of MO with BTO, Fe-BTO, and Pt/Fe-BTO, respectively, is noted. Stability analysis indicates that a mild oxidative treatment at 350 °C is sufficient to recover ~86% of the photoactivity lost over 6 h of exposure to photoillumination in 2 h increments. Further, for the first time, complementary photoelectrochemical and optical measurement tools have been used to systematically probe the functioning of BTO in the presence of Fe and Pt. Electrochemical impedance, chronopotentiometry (intermittent illumination studies), and fluorescence measurements reveals (i) Fe aids in visible light assisted charge separation, (ii) Pt is not as effective with visible light as it is with UV, and (iii) a high concentration of hydroxyl radical in the Pt/Fe-BTO is the basis for improved photoactivity of the catalysts. Using bismuth titanate pyrochlore as a case study, this work demonstrates the approach to leverage optical and photoelectrochemical tools for systematic analysis of other multi-metal oxides that belong to the sillenite, delafossites, pyrochlores, and scheelites.

1. Introduction

Solar-driven environmental remediation of pollutants has traditionally been performed with oxide photocatalysts that consist of a single metal ion compounds as a base material – such as Ti in TiO_2 [1–3]. To improve the oxides' ability to facilitate enhanced photocatalytic remediation of environmental pollutants, a combination of oxide with other metal ions, zero-valent metal ad-atoms, metal oxides, or other photoactive entities, has been extensively studied [4,5]. These combinations can allow for enhanced (i) light absorbance [6], (ii) charge separation [7,8], and/or (iii) broad band absorbance,[9] leading to improved photoactivity. Unlike single metal oxides, the multi-metal oxides such as delafossite, sillenite, perovskites, or pyrochlores consist of structures that offer a unique benefit – the option to include additional elements (not including doping) [10,11]. The primary benefit with this option is the realization of an additional degree of freedom to include one or more additional element(s) that can aid with tuning the optical, electronic, and/or the photocatalytic properties [12]. The choice of elements in the structure can alter the bandgap, direct/indirect properties, and the light mediated surface redox reactions.

Several mixed oxides have been tested in photocatalysis with their noteworthy applications in the areas of solar fuel generation and environmental remediation [13–16]. As a case study, we have examined the synthesis of a pyrochlore photocatalyst comprising of Bi and Ti as the primary elements [17]. Choosing Ti as the element for the B site, allows for the 3d orbitals to define the conduction band. On the same note, Bi as the element in the A site allows for establishing the valence band along with the O 2p orbital. This combination is unique because the overall bandgap is determined to be 2.6 eV (Scheme 1) and it offers the possibility to perform wide ranging photocatalytic reactions and if needed, with visible light excitation as well. In previous works, we have evaluated the application of the BTO pyrochlore as a hydrogen evolution photocatalyst with water-methanol mixtures [18,19].

In a related study Yao et al., have shown that rare earth element such as La can promote the photodegradation of textile dye using bismuth titanate [20]. A rigorous density functional theory study, or

* Corresponding author.
E-mail address: ravisv@unr.edu (V.R. Subramanian).

http://dx.doi.org/10.1016/j.apcatb.2015.06.016
0926-3373/

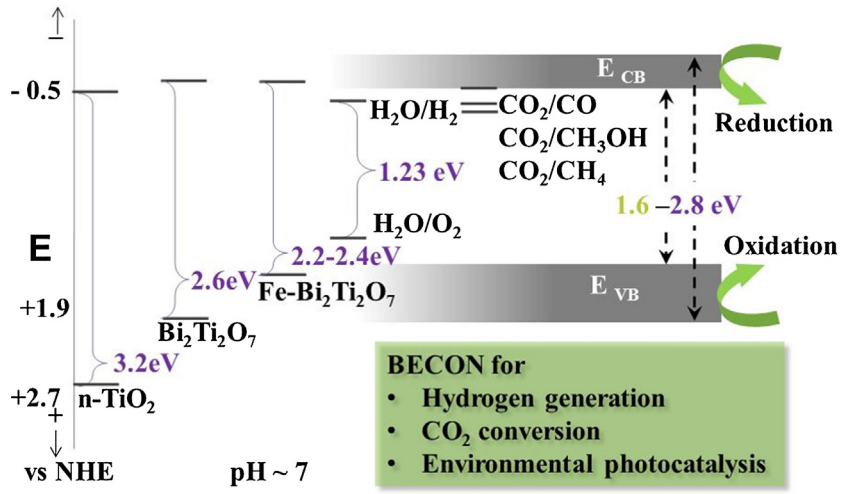

Scheme 1. The energy band-edge positions of the bandgap engineered composite oxide nanostructures –BECONs – relative to the global standard TiO_2 is shown. The redox potential of reactions of interest to solar – driven photocatalytic processes is also shown indicating the potential multi-functionality of the BECONs.

DFT analysis, on pyrochlore BTO and a series of elements belonging to the 3d group has determined that inter-band states can be created in the BTO that will affect optical absorbance [12]. Since these multi-metal oxides offer a bandgap tunability option, we refer to these compounds as bandgap engineered composite oxide nanostructures or BECONs. We have validated the modeling predictions by showing that pyrochlore BECONs containing earth abundant 3d elements such as Fe, Mn, Co, or Ni can promote the photoactivity of BTO and also showed preliminary experimental results demonstrating the benefits of such 3d element addition to BTO [12,21]. Though these preliminary modeling results are promising, several aspects of BTO based multi-element BECONs still remain to be fully understood. Before exploring the applicability of other elements as building blocks by following a rather Edisonian pathway, one has to understand (i) how does the inclusion of a 3rd element in these BECONs comprising of earth abundant elements, influence the environmental remediation aspect of the BTO, (ii) how does the addition of external ad-atoms to this mix, a highly beneficial step for single metal oxides, influence photoactivity, and (iii) if it is possible to explain the activity of these catalysts using photoelectrochemical techniques.

In this work, we report on the application of BTO composite with Fe as a case study for the remediation of an environmental pollutant methyl orange, to answer the aforementioned questions. Firstly, the optimization of the Fe-BTO photoactivity has been performed by examining catalyst loading and dye concentration effects. Secondly, the improvement in the photoactivity of this Fe-BTO BECON due to the addition of a co-catalyst, Pt, a well-known promoter of photoactivity, has been examined, under the optimized experimental conditions. Thirdly, the photoactivity of the BECONs upon sustained use has been examined by performing repeat experiments to correlate surface properties with photoactivity. To determine application potential, the activity of all photocatalysts has also been examined under 100% visible light illumination. Finally, we have performed optical and photoelectrochemical studies to understand and correlate the interfacial relative oxidative properties of all the photocatalysts.

2. Experimental

2.1. Materials

The synthesis was carried out using precursor chemicals obtained from local suppliers. Nitric acid ACS, BDH3046-2.5LPC, 68%, (BDH Aristar), bismuth nitrate pentahydrate (ACS, 98%, Alfa Aesar), titanium (IV) isopropoxide (97%, Sigma–Aldrich), Iron(III) nitrate nonahydrate (ACS, >98%, Sigma–Aldrich), and ammonia solution (A667-212, >25%, Fisher Scientific) were all purchased from the commercial vendors respectively. Stock solutions of 1 M Nitric Acid, 0.1 M bismuth nitrate, 0.1 M titanium isopropoxide, and 0.1 M iron nitrate were prepared. Deionized water from Millipore® system was used to dilute and wash all precipitates formed.

2.2. Photocatalyst synthesis

0.1 M solution of each of the precursors were taken in an acidified medium (HNO_3 as solution) and mixed together in stoichiometric proportions as shown in the supplementary information, Fig SI 1. After thorough mixing for 10 min the pH of the solution was changed by the addition of ammonium hydroxide leading to the formation of a yellowish–white solid precipitate. The solid was ground into a fine powder and mildly heat treated to remove high volatile organics. High temperature thermal treatment was then performed at 600 °C for 6 h to facilitate phase transformation. In the experiments involving Pt, Pt was deposited by photo-reduction of an aqueous Pt salt solution of chloroplatinic acid hexahydrate (H_2PtCl_6, $6H_2O$), by irradiation in the presence of the Fe_BTO.

2.3. Surface analysis

Phase analysis of the photo-catalysts was carried out using XRD [A Philips (model: 12045 B/3X-ray diffractometer) instrument with Cu K-alpha as X-ray source]. The surface analysis was performed using optical spectroscopy and photoelectrochemistry measurement tools. SEM (Hitachi® S-4700) was used to examine the physical features of the oxide nanoparticles. TEM (JEOL® 2100F) was used to determine the particle size. Optical absorbance measurements were performed using a UV–vis spectrophotometer (Shimadzu® UV-2501PC) to determine the photocatalysts stability before and after usage. Films of the photocatalyst were prepared on conducting glass slides for photoelectrochemical (PEC) measurements. These measurements were performed on the photocatalyst film using an Autolab Potentiostat/Galvanostat to gather chronoamperometry and chronopotentiometry data [22]. A Xenon lamp was used as the light source in an optical train consisting of a setup detailed elsewhere [23].

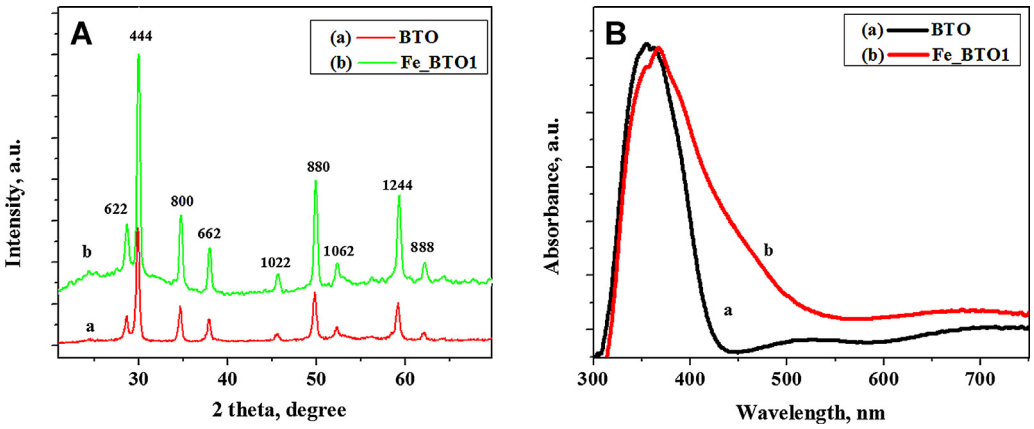

Fig. 1.

2.4. Photocatalysis experiments using slurry reactor set-up

The photoactivity of the Fe-BTO, with and without Pt, was examined using a 500 mL slurry reactor with a jacketed cooling option. A pyrex reactor was used and its assembly is described elsewhere [24]. A 250 mL of an aqueous solution of methyl orange with concentrations of 10 and 20 μM was used as the model pollutant. A Xe lamp with a 300 W output power was used as the light source in all experiments. In the case of the visible light mediated photocatalytic dye-degradation experiment, a FRS-GG400 filter from Newport® and 0.5 M $CuSO_4$ solution was used in the light source to cutoff the UV region. The changes to the irradiated solution were noted using spectroscopy at regular intervals of time. All solutions were irradiated in an oxygen environment. The photocatalysts were decanted, dried, and reused to determine the extent of their reactivity. All photocatalytic experiments were performed in duplicate to ensure reproducible trends. The catalysts are labelled as BTO (Bismuth titanate -$Bi_2Ti_2O_7$), Fe_BTO1 (1 wt% iron modified $Bi_2Ti_2O_7$), and Fe_BTO_Pt (Fe_BTO1 with Pt at the surface).

3. Results

3.1. Structural and compositional characterization of the photocatalyst

Fig. 1A shows the XRD of the synthesized photocatalyst. The XRD peaks are indexed using the JCPDS Card # 32-0118. The peak at 28.7° corresponds to the 622 plane and 29.9° corresponds to the 444 plane of BTO. Fig. 1B shows the absorbance spectra of Fe-free BTO and 1% Fe_BTO. A significant red-shift is observed, indicating that the presence of iron within the BTO enhances the visible light absorption through a shifting of the onset absorbance by approximately 100 nm. This shift into the visible region is a critically desirable component when developing and designing visible light activated photocatalysts. The bandgap was calculated from the UV–vis spectra using the relationship $E = hc/\lambda$, applied at the onset. The shift in the onset of absorbance has the equivalent effect of reducing the energetics by 0.4 electron volts from approximately 2.8 eV to 2.4 eV. This trend of enhancing visible light absorbance with a third element addition is in agreement with earlier results obtained using pseudo-plane wave density function modeling studies on these types of multi-metal oxide photocatalysts [12,25]. Of noteworthy importance from the XRD analysis is that the catalysts prepared with 1% Fe do not show any Fe-based oxide suggesting that the Fe is a part of the BTO. Fig. 2A and B shows the SEM and TEM images respectively of the 1% Fe_BTO. Further, the SEM indicates that the physical shapes of the particles are similar and they are well dispersed (not aggregated).

The TEM provides a discernable image of the catalyst features and the size measurement indicates an average diameter of 10 ± 4 nm. Most of the nanoparticles show the crystalline Fe-BTO phase. On a closer examination of some of the nanoparticles, localized amorphous regions can be noted. This could be Fe oxides, such as Fe_2O_3 or Fe_3O_4. Therefore, they have been labelled as Fe_xO_y. These regions are indicated with circles in the TEM in Fig SI_2). Further, the TEM image obtained after metal deposition shows nanoparticles dispersed on the oxide surface existing in close proximity as shown in Fig. 3A. Broad area EDAX analysis confirms the

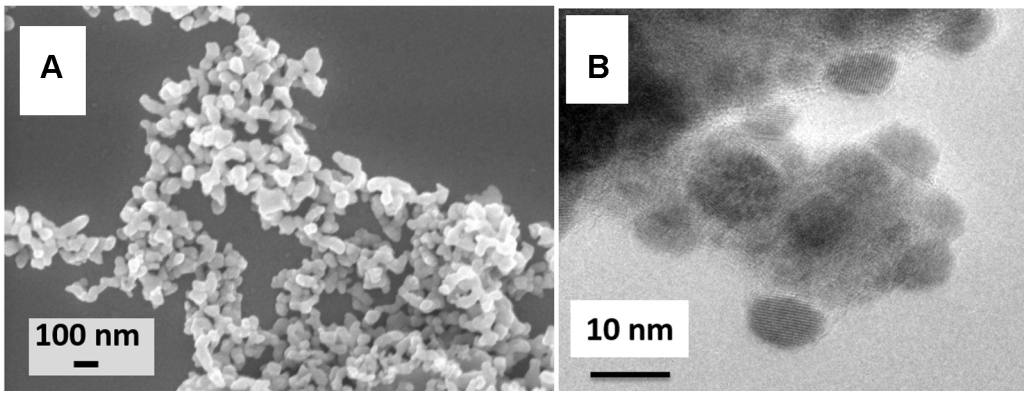

Fig. 2.

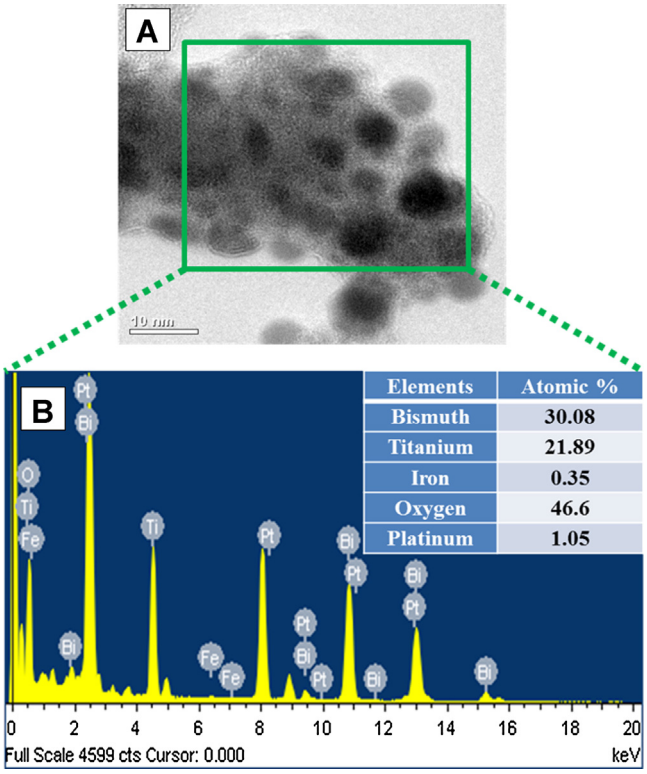

Fig. 3.

presence of these deposits as Pt nanoparticles as indicated in the inset of Fig. 3B.

3.2. Optimization ***of the catalysts'*** photoactivity

3.2.1. Effects of the catalyst loading on MO conversion with Fe-modified BTO.

MO is a complex organic molecule that is often used as a textile dying agent. MO has been chosen as a standard model-dye to verify the photocatalytic performance of various synthesized catalysts since its degradation using different photocatalysts have been well researched and its degradation products are well characterized [26–29]. The effect of catalyst loading on the photo-conversion of the MO was examined at a dye concentration of 10 μM. 5 mL aliquots of the dye were removed from the slurry reactor and the absorbance was checked at regular time intervals. A consistent decrease in the peak absorbance of the dye at ~450 nm was noted over time (Fig. SI_3), without any additional peak formation. Control experiments with the dye in the catalyst absence (Fig. SI_4) indicates no degradation of MO, demonstrating that dye photolysis does not occur and the catalyst is instrumental in effecting the conversion of the dye. In addition to that, before photocatalysis, we have carried out dark runs, [with catalyst (no illumination) in the dye solutions] for a period of 4 h to verify if any adsorption occurs. This control experiment shows that (Fig. SI_5) an insignificant absorption takes place for an initial ~1 h and after that no adsorption takes place ($C_t/C_o = 0.99$). Therefore, prior to performing the photodegradation experiments, an initial dark run was conducted for ~2 h to ensure absorption occurs. At this point concentration was initialized to C_O.

Fig. 4**A** shows a plot of the conversion of the dye against time for different catalyst loadings. The conversion was calculated from the absorbance spectra and normalized to the initial concentration. It can be noted that more photocatalysts indeed favor MO degradation. If more photocatalyst is present within the system then more electron–hole pairs are generated upon photo-illumination. The additional holes are essential for increased production of [$OH^•$] radicals in the solution to improve the degradation of the dye molecules. This linear increase is noted up to a critical loading of the catalyst in the reactor system, after which there is a decrease in overall conversion. The decrease may be attributable to the light-scattering effect of the catalyst. An optimal loading of 150 mg is noted to be most effective for this system, facilitating a ~53% dye conversion over a 2 h period.

3.2.2. Effects of the dye concentration on the photoactivity of the Fe-modified BTO

The effect of the dye concentration was examined at the optimal loading of 150 mg. Increasing the dye concentration from 10 μM to 20 μM demonstrated a decrease in the conversion of the dye over a 2 h period as shown in Fig. 4**B**. This observation may be attributed to light screening effect of the dye, and/or reduced availability of active catalyst sites for MO molecules for adsorption and reaction [30]. Further, it has been noted that in both dye concentration experiments, the presence of Fe yields a higher conversion of the dye compared to Fe-free BTO. The increased activity with the Fe presence is attributed to the greater visible light absorbance, which leads to more e–h pair generation, proving that Fe addition is beneficial.

3.3. Boosting the performance of the photocatalyst with Pt addition

It is well known that the addition of metals such as platinum or gold as a co-catalyst can improve the photocatalytic activity of single metal oxides as indicated with the extensive studies with TiO_2 [31,32]. The improvement in activity is attributed to the ability of the metal to aid in separation of charges which promotes hole availability for oxidative reactions [6,7,33]. Pt was added to the Fe-BTO to examine the co-catalyst effect on MO oxidation. The time resolved photographs indicate an almost complete loss of color of the dye after illumination (Fig. 5**A**). At a Pt loading of ~1 wt%, the photoactivity of the Fe-BTO was noted to increase by ~88% within the 2 h illumination period as shown in Fig. 5**B**. Such a boosting effect confirms that the co-catalyst activity, noted with single metal oxides, is also observed with multi-metal oxides, and that the Pt functions as an electron sink leading to the freeing up of more holes that promote the oxidation of MO.

3.4. Kinetic analysis of the photoactivity of Fe-BTO and Pt/Fe-BTO

The kinetics of the MO conversion was analyzed using a pseudo steady state first order lumped parameter model [11,23]. The rate constant of the reaction were determined by linearization of the conversion data shown in Figs. 4 and 5**B**. Fig. 6 summarizes the corresponding rate constants (Fig. SI_6 shows the results of linearization) for each of the experiments. The values are of the order of 10^{-3} min^{-1}, with the maximum rate constant observed for the degradation of MO using Fe-BTO in the presence of the Pt deposits. The trends in the results are consistent with those noted in earlier reports [23,30]. From a mechanistic standpoint, the fact that the dye absorbance decreases monotonically, suggests that the MO degradation process on Fe-BTO and Pt/Fe-BTO follows an established mechanism discussed elsewhere [29,34].

3.5. Stability of the photocatalysts

The photocatalysts' were recovered after the first 2 h run by centrifugation and then subjected to drying. They were used with a fresh solution of the dye and tested for another 2 h for their activity. Fig. 7**A** shows the fractional conversion of the dye after 3 such

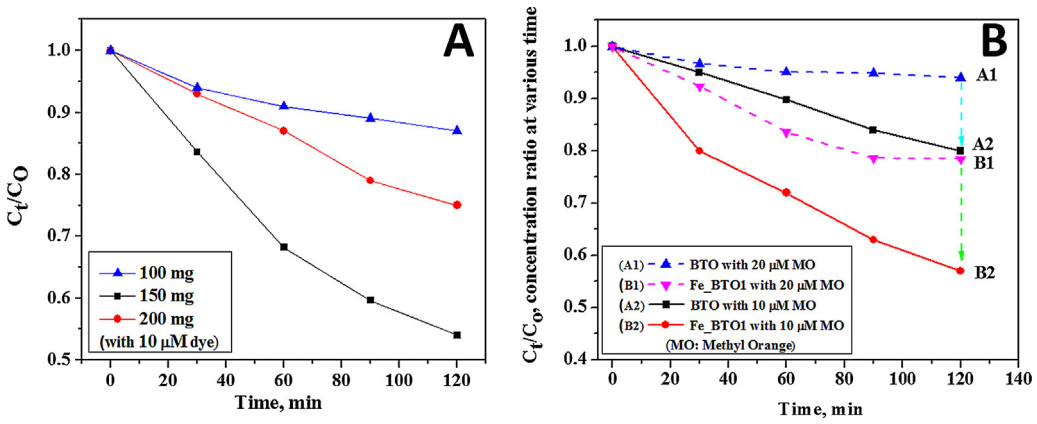

Fig. 4.

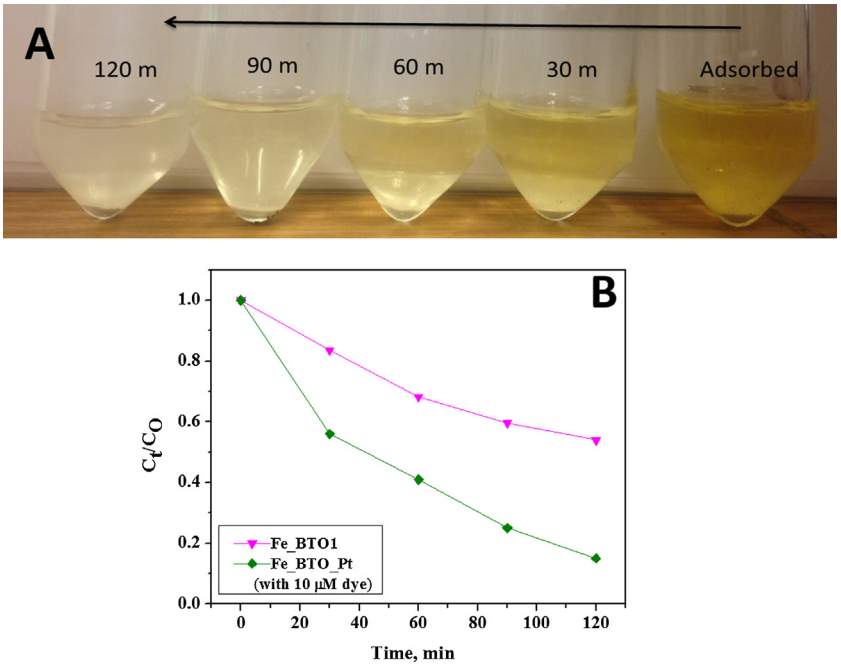

Fig. 5.

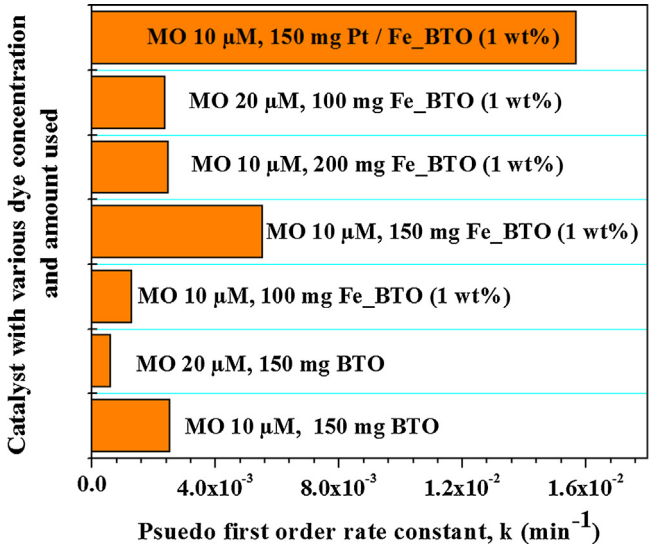

Fig. 6.

repeated runs over a 6 h period. The second and the third runs show a progressive decrease in the fractional conversion of the dye. Absorbance spectra of the used photocatalyst is shown in Fig 7**B**. Images of the photocatalysts before and after MO conversion show a change in the coloration (Fig. 7**C**). For recovery studies, the catalyst was subjected to a mild thermal oxidative treatment at 350 °C. When this treated photocatalyst was used again for MO conversion (Fig. 7**A**, "recovered"), the recovery in the activity becomes evident. The absorbance spectra of the treated photocatalyst (Fig. 7**B**) also show a profile similar to the unused photocatalyst. This recovery of the photoactive sites can be attributed to the oxidative removal of intermediates produced and deposited during the photocatalysis. Thus, the reason for the decrease in the degradation efficiency of the photocatalyst on repeated use is attributable, at least in part, to the surface adsorbed species (any possible catalyst instability effects has to be further examined). In related literature, alternate approaches such as photo-irradiation, thermal treatment, or chemical treatment have also been reported for recovery of activity [35,36]. For example, an alternate non-thermal approach could involve the use of mild oxidative surface treatment methods such as aqueous H_2O_2 digestion, to remove the surface organics.

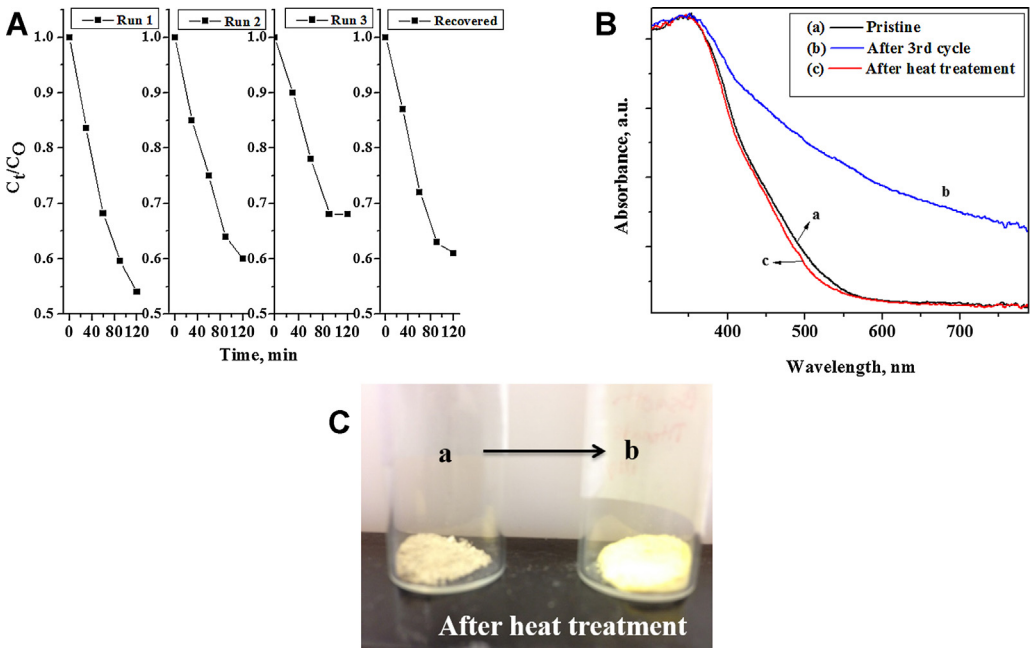

Fig. 7.

3.6. Visible light activity

The visible light activity of the catalysts was examined using UV cut-off filters (discussed in Section 2) in the path of the light source. A 2 h continuous illumination indicates a fractional conversion of 10%, 15%, and 21% of the dye in the presence of BTO, Fe-BTO and Pt/Fe-BTO, respectively. This activity can only be possible due to the visible light photons absorbed by the presence of Fe (as discussed earlier in Section 3.1, Fe-BTO showed a 100 nm red-shift in the absorbance, compared to BTO). Of noteworthy importance is the result that the presence of Pt offers only an improvement of 40% and Pt is also as effective as it is under UV–vis illumination (~88%, Section 3.3). However, without Fe a significant amount of conversion can be noted with Pt as well. This indicates that, the presence of Fe is clearly not the sole reason for the improved activity, rather the presence of Fe and Pt, together, synergistically aid in improving the photoactivity. In a related work, the visible light-driven MO photodegradation has been demonstrated with Bi–Fe–Nb composites.[37] The choice of Nb establishes a higher level conduction band compared to Ti. Thus, our work and this literature, suggest that 100% visible light driven activity is possible with Fe inclusion, and is a step in the right direction toward visible light active photocatalyst design. However, further studies need to be undertaken by considering the inclusion of other elements within the BTO.

4. Discussions

The role of Fe in promoting visible light photocatalytic activity of oxides has been addressed in the past investigations [38–42]. Theoretical and experimental studies suggest that Fe inclusion in oxides such as TiO_2 (single metal oxide) generally lead to the creation of inter-band states which reduces the effective bandgap and thereby aids in improving absorbance in the visible region [40]. Alternately, in a model multi-metal oxide, based on our earlier DFT-based modeling investigations we have demonstrated that 'Fe' inclusion (in bismuth titanate-$Bi_2Ti_2O_7$) causes a more visible light absorbance through formation of inter-band states because of Fe^{3+} [12]. The increased photocatalytic activity can also be attributed to charge trapping effect of Fe^{3+} which enhances the lifetime of photogenerated charge carriers [40,41]. Likewise, when it comes to ad-atoms such as Pt addition outside of the pyrochlore framework, it is known that the zero-valent metal acts as an electron sink [8,11,43–45]. That is, upon photo-illumination the metal accepts the electrons and enhances the hole lifetime of an oxide. Thus, based on these inferences, the role of Fe within the pyrochlore matrix and Pt present as ad-atom can be attributed to facilitating improved e-h separation and allowing the hole to become available for oxidative processes. In the earlier section the (i) surface features, (ii) photocatalyst absorbance features, (iii) systematic optimization of the photoactivity of BTO and Fe-BTO in the presence of UV–vis and visible light, and (iv) the effect of Pt addition, has been presented. Therefore, this section focuses on the use of applied tools such as photoelectrochemical techniques and fluorescence analysis to provide additional insights into the performance of the various photocatalysts' upon illumination.

4.1. Photoelectrochemical insights

Photoelectrochemical or PEC measurements provide insights into the effects of the application of external driving forces, such as potential, on the transport of charges within photocatalyst films [46]. The PEC measurements of the photocatalysts, immobilized on ITO-coated conducting glass slides, were performed using a 0.1 M sodium hydroxide (NaOH) solution as electrolyte. The chronopotentiometry (V/t) responses of the films under periodic on-off illumination were performed to determine the rapidity of charge separation in the photocatalyst.

Fig. 8**A** indicates the instantaneous response to illumination. A step function response shows that electron–hole pairs are instantaneously generated and remain separated. A control experiment with a TiO_2 film was also performed (shown in Fig. SI_**7**). It indicates the typical n-type characteristic with the increasing voltage. Further, MS analysis was performed using the BTO film. Contrasting the result from the BTO experiment with the TiO_2 control and the MS analysis, it can be concluded that the BTO demonstrates n-type characteristics. Since Fe_BTO comprises of earth abundant elements and can be prone to corrosion, extended illumination

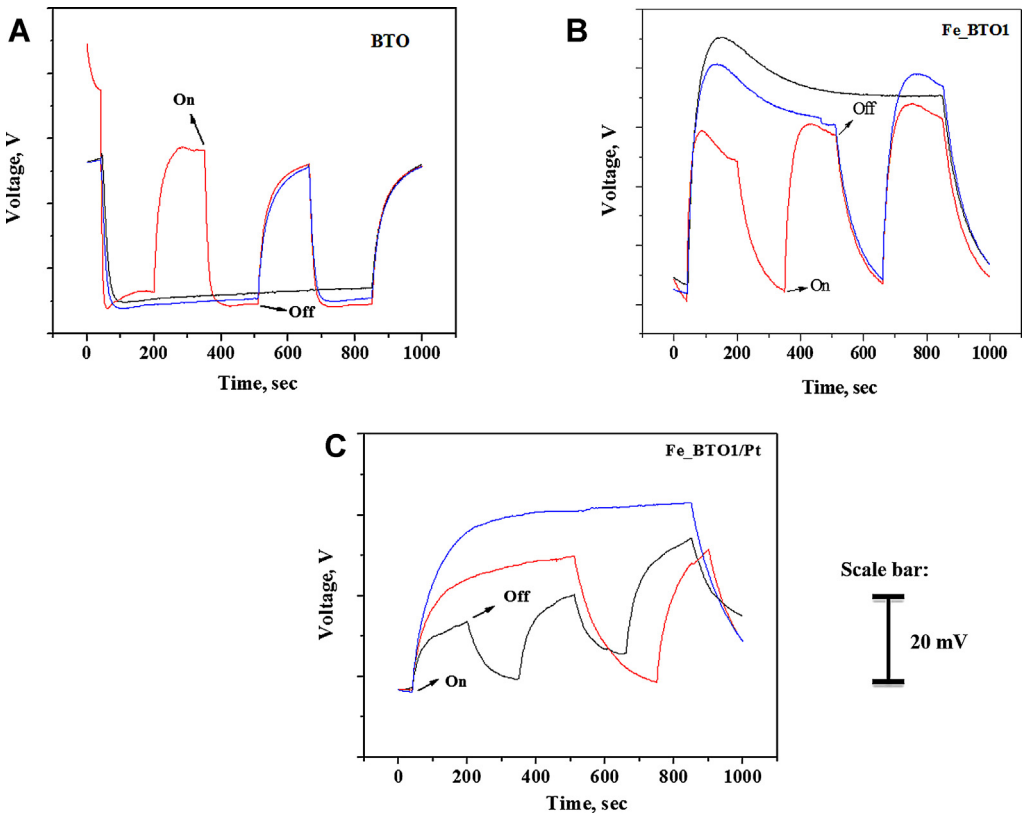

Fig. 8.

Table 1
ΔV [measured from Chronopotentionmetric (V vs t) analysis] and Fluorescence signal intensity [of 2-hydroxyterephthalic acid (TAOH), measured at 426 nm for the] for various photocatalysts, BTO, Fe_BTO (1 wt% Fe) and Fe_BTO with Pt.

Sample	ΔV, (V)	Fluorescence intensity (A.U.)
BTO	0.043	18,97,404
Fe_BTO (1 wt%)	0.046	19,77,680
Pt/Fe_BTO (1 wt%)	0.048	33,24,546

effects was also examined. Continuous illumination of the film shows an almost constant voltage of ~45 mV indicating that the response is because of the photogenerated electrons. This result along with the absorbance of the photocatalyst shows that the BTO synthesized by the method presented here is not prone to structural destabilization by corrosion.

The V/t response of the Fe modified BTO presented in Fig. 8**B** shows three interesting responses. Firstly, the direction of the flow of current is opposite to the direction noted with BTO. This indicates that the presence of Fe makes the Fe-BTO display a p-type characteristic. Secondly, though the response to continuous on-off cycles is instantaneous, unlike BTO films the magnitude of the voltage is not constant and gradually increases. However, continuous illumination suggests that the voltage passes through a maximum and then stabilizes as shown in Fig. 8**B**. Finally, the decay of the voltage is also relatively much slower compared to the BTO. These observations indicate that Fe is playing a role in the movement and trapping/de-trapping of the photogenerated electrons. The results with Pt deposits on the Fe-BTO are shown in Fig. 8**C**. The responses are identical to the results seen with Fe-BTO in Fig. 8**B.** Interestingly, the voltage does not pass through maxima as evident with Fe-BTO. The ΔV associated with each of the films containing the Fe or Pt is ~15% higher than the one noted with BTO as indicated in Table 1.

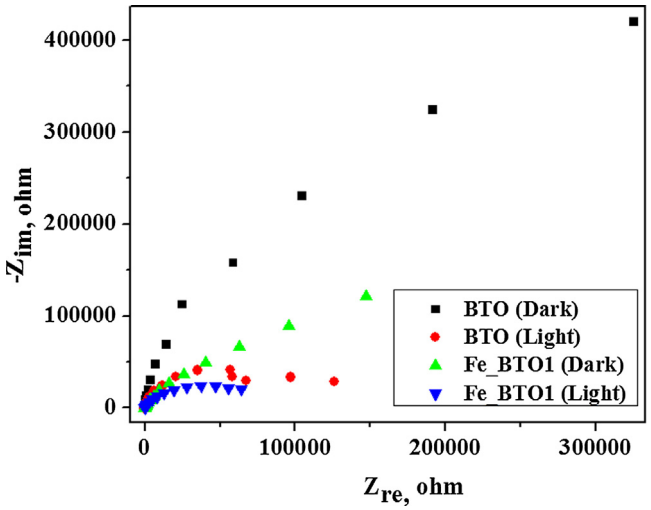

Fig. 9.

4.2. Electrochemical impedance analysis

The electrochemical impedance spectroscopy (EIS) measurements offer insights into the effectiveness of the photocatalyst to separate the photogenerated charges [47,48]. The EIS measurement was performed using the photocatalyst films prepared on conducting glass (ITO) in the presence of aqueous Na_2SO_4. A plot of the imaginary and real coordinates for the films in the presence and absence of photoillumination is shown in Fig. 9. The greater the radius of the arc, the lower the extent of interfacial charge transfer occurring within the system [47]. A comparison of Fe_BTO with the BTO indicates that the charge separation is greater with Fe_BTO than BTO, attributable to the Fe presence. The increased activity

of the BTO observed in the results section can be correlated to the improved charge separation resulting in greater availability of holes for oxidation.

A similar observation was noted in earlier studies on single metal oxide photocatalysts involving Fe doped TiO_2 [49] and Fe doped graphitic C_3N_4 [50]. The other factor that could be playing a role in the charge separation is Fe functioning as a center for trapping photo generated electrons (evident from the reduction in the photovoltage). With this phenomena a likely possibility, the holes are still available for promoting the oxidative process. In fact, the observations using impedance and chronopotentiometry measurements indicate a beneficial role of the Fe presence. It should be pointed that, we cannot isolate a generic link between charge separation and rate limiting step. This is because, other parameters such as light intensity, catalyst loading, screening effects of the dye are well – known physicochemical parameters which can definitively impact rate limiting step [30,51,52].

4.3. Probing of •OH concentration using fluorescence

The hydroxyl radical (•OH) is a strong oxidizing intermediate that aids in environmental remediation [53]. Its formation, via $h^+ + OH \rightarrow$ •OH, is critical to the initiation of the oxidative mineralization of the MO [54]. Therefore, probing its concentration in the presence of various photocatalysts (BTO, Fe-BTO and Pt/Fe-BTO) will provide additional insights into how the presence of Fe and Pt influence •OH availability under illumination. The formation of the reactive •OH can be tracked using terephthalic acid (TA) as a probe in fluorescence spectroscopy [55,56]. In this experiment, the photogenerated •OH react with terephthalic acid (TA) and forms a fluorescent 2-hydroxyterephthalic acid (TA-OH). In a typical experiment, the photocatalyst is mixed in a basic TA solution (in water) and then charged with the same light source used for the photodegradation experiment. The emission spectrum (measured at 424 nm) corresponding to TA-OH was measured after a time interval of 45 min. Table 1 shows the relative fluorescence signal intensities of the TA-OH generated during the course of the reaction with various catalysts. The intensity follows the order: Pt/Fe-BTO > Fe-BTO > BTO, indicating that the largest amount of hydroxyl radicals is generated in the presence of Pt/Fe-BTO. This observation confirms that the holes are produced and available at its highest level in the presence of Fe and Pt and validates the trends in the photocatalysis studies.

4.4. Insights into the mechanism of charge trapping /de-trapping in the Fe-BTO and Pt/Fe-BTO photocatalyst

From the observations in the results and discussion sections, the photo-generated charge trapping/de-trapping in Fe-BTO and Pt/Fe-BTO can be summarized as illustrated in the Scheme 2. The absence of Fe or Pt leaves the BTO as an ineffective photocatalyst due to severe charge recombination (**2a**). The presence of Fe in the Fe-BTO imparts a beneficial effect in the photocatalytic degradation of MO by (i) serving as a 'localized' electron-trap center and (ii) promoting enhanced hole mediated photodegradation of MO compared to BTO (**2b**). The former aspect of Fe presence was probed using light-induced photovoltage measurement as a function of time. The electron trapping phenomena in Fe-BTO is indicated from the decay characteristic of the photovoltage, after reaching a peak value under constant photo-illuminated condition. This critical response is reproduced in the multiple on-off cycles of the photovoltage vs time trace. The electron-trapping phenomenon prevents the electron–hole recombination and enhances the hole lifetime for oxidative reactions to generate higher •OH concentration, compared to BTO. The increase in the reactive •OH concentration was indicated from the terephthalic acid or TA experiment (discussed in Section 4.3).

Furthermore, Pt (noble metal) deposition at the Fe-BTO surface results in the buildup of the voltage, after photoillumination, as indicated in Fig. 8**C**. This specific behavior is due to the electron accumulation at the surface 'Pt' centers, acting as '*electron-sink*'. This, effect is further beneficial for photo-remediation, as it boosts the hole-lifetime and significantly increases the reactive OH concentration (probed using TA experiment) compared to Fe-BTO, which is responsible for a greater MO degradation. A more roundabout mode for hydroxyl radical generation using the electrons trapped in Pt can occur via a superoxide anion (**2c**). However, this contribution is predominant only under UV–vis illumination (~30%) compared to visible illumination (~6%).

Finally, the Fe addition to BTO raises two further questions: (1) How does Fe present as Fe_xO_y at the BTO-oxide surface (note that the absence of Fe_xO_y peaks in the XRD cannot conclusively rule out a very small Fe_xO_y content) impact photocatalyst performance? and, (2) What is the site in which the Fe is incorporated (Bi- or Ti-) and how does it affect performance? Even if there is Fe_xO_y presence on the surface, Fe_xO_y is limited in its ability to contribute to photoactivity by itself (very high recombination rates); it has to coexist with another catalyst with straddled band energetics [57,58]. This aspect has to be probed using HRTEM. In the case of the latter, further studies (for example using EXAFS/XANES) are required to probe the structural form of Fe_BTO studied in this work. This structural analysis will aid in further understanding of the photoactivity of these composites.

5. Conclusion

This work presents a detailed analysis of the photocatalytic activity of a pyrochlore photocatalyst comprising of earth-abundant elements, Bi, Ti, Fe, and O in the form of bismuth titanate (BTO and Fe-BTO) as well as the effects of Pt addition as a co-catalyst. A series of inter-related studies involving the evaluation of the effects of catalyst loading, light intensity, dye concentration, and the decoupling of the visible and UV light effects – physicochemical factors that underline the performance of the photocatalyst – have been systematically investigated using a slurry-based reactor configuration. Photoelectrochemical analysis performed using impedance measurements (EIS) and photovoltage (V/t), for the first time, sheds light into the role of Fe as a center promoting the separation and trapping of photogenerated charges in the Fe-BTO and Pt/Fe-BTO systems. Further, from a photocatalyst stability standpoint, repeated use indicates a continued reduction in the photocatalyst performance in subsequent cycles. A simple post-use oxidative treatment is very effective in purging out these groups without imparting any detrimental transformation in the optical and/or physical features of the photocatalyst. This work sets the protocol for the systematic and detailed testing of other forms of multi-metal oxides such as delafossites, sillenite, spinels, or perovskites in photo-driven environmentally relevant catalytic reactions.

Acknowledgements

R.S.V. gratefully acknowledges National Science Foundation funding (NSF-CBET 1134486). R.S.V. would like to thank Cashman Equipment for supporting the graduate studies of W.R. Support for research from the Undergraduate Research Office at UNR for S.D. and K.C. is also acknowledged.

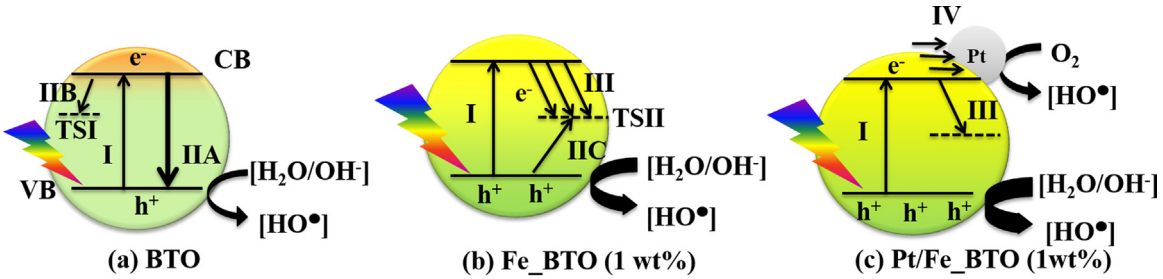

VB: Valence Band
CB: Conduction Band
TSI: Trap-sites within BTO
TSII: Trap-sites created predominantly by Fe^{3+} in Fe_BTO1
I: Photo-excitation and e-h pair formation
IIA/B/C: Recombination of the electron with hole
III: Recombination of the electron in the trap site created by Fe^{3+}
IV: Charge separation at the oxide/Metal interface
•OH: Hydroxyl radical

Scheme 2.

Appendix A. Supplementary data

Supplementary data associated with this article can be found, in the online version, at http://dx.doi.org/10.1016/j.apcatb.2015.06.016

References

[1] K. Pirkanniemi, M. Sillanpaa, Chemosphere 48 (2002) 1047–1060.
[2] E. Pelizzetti, C. Minero, Electrochim. Acta 38 (1993) 47–55.
[3] A. Mills, R.H. Davies, D. Worsley, Chem. Soc. Rev. 22 (1993) 417–425.
[4] J. Chen, D.F. Ollis, W.H. Rulkens, H. Bruning, Water Res. 33 (1999) 1173–1180.
[5] M.R. Hoffmann, S.T. Martin, W.Y. Choi, D.W. Bahnemann, Chem. Rev. 95 (1995) 69–96.
[6] W.Y. Choi, A. Termin, M.R. Hoffmann, J. Phys. Chem. 98 (1994) 13669–13679.
[7] V. Subramanian, E.E. Wolf, P.V. Kamat, Langmuir 19 (2003) 469–474.
[8] V. Subramanian, E.E. Wolf, P.V. Kamat, J. Phys. Chem. B. 105 (2001) 11439–11446.
[9] S.C. Lo, C.F. Lin, C.H. Wu, P.H. Hsieh, J. Hazard. Mater. 114 (2004) 183–190.
[10] L.L. Garza-Tovar, L.M. Torres-Martinez, D.B. Rodriguez, R. Gomez, G. del Angel, J. Mol. Catal. A – Chem. 247 (2006) 283–290.
[11] V. Subramanian, R.K. Roeder, E.E. Wolf, Ind. Eng. Chem. Res. 45 (2006) 2187–2193.
[12] S. Murugesan, M.N. Huda, Y. Yan, M.M. Al-Jassim, V. Subramanian, J. Phys. Chem. C 114 (2010) 10598–10605.
[13] W.F. Yao, H. Wang, X.H. Xu, J.T. Zhou, X.N. Yang, Y. Zhang, S.X. Shang, Appl. Catal. A: Gen. 259 (2004) 29–33.
[14] J. Zeng, H. Wang, Y.C. Zhang, M.K. Zhu, H. Yan, J. Phys. Chem. C 111 (2007) 11879–11887.
[15] S.H. Xu, W.F. Shangguan, J. Yuan, J. Shi, M.X. Chen, Mater. Sci. Eng.: B 137 (2007) 108–111.
[16] Y. Yang, Y.B. Sun, Y.S. Jiang, Mater. Chem. Phys. 96 (2006) 234–239.
[17] S. Murugesan, V. Subramanian, Chem. Commun. (2009) 5109–5111.
[18] S. Gupta, V. Subramanian, ACS Appl. Mater. Interfaces 6 (2014) 18597–18608.
[19] S. Gupta, L. Leon, V. Subramanian, Phys. Chem. Chem. Phys. 16 (2014) 12719–12727.
[20] W.F. Yao, H. Wanga, X.H. Xua, X.N. Yanga, Y. Zhanga, S.X. Shangc, M. Wanga, Appl. Catal. A – Gen. 251 (2003) 235–239.
[21] B. Allured, S. DelaCruz, T. Darling, M. Huda, V. Subramanian, Appl. Catal. B-Environ. 144 (2014) 261–268.
[22] V. Subramanian, Interface 16 (2007) 32–36.
[23] V. Subramanian, P.V. Kamat, E.E. Wolf, Ind. Eng. Chem. Res. 42 (2003) 2131–2138.
[24] V. Jaeger, W. Wilson, V. Subramanian, Appl. Catal. B: Environ. 110 (2011) 6–13.
[25] A. Kudo, H. Kato, S. Nakagawa, J. Phys. Chem. B 104 (2000) 571–575.
[26] D. Ansorgova, M. Holcapek, P. Jandera, J. Sep. Sci. 26 (2003) 1011–1027.
[27] A. Plum, A. Rehorek, J. Chromatogr. A 1084 (2005) 119–133.
[28] T. Chen, Y. Zheng, J.M. Lin, G. Chen, J. Am. Soc. Mass Spectrom. 19 (2008) 997–1003.
[29] C. Baiocchi, M.C. Brussino, E. Pramauro, A.B. Prevot, L. Palmisano, G. Marci, Int. J. Mass spectrom. 214 (2002) 247–256.
[30] Y. Smith, A. Kar, V.R. Subramanian, Ind. Eng. Chem. Res. 48 (2009) 10268–10276.
[31] H. Lachheb, E. Puzenat, A. Houas, M. Ksibi, E. Elaloui, C. Guillard, J.M. Herrmann, Appl. Catal. B-Environ. 39 (2002) 75–90.
[32] V.M. Daskalaki, M. Antoniadou, G. Li Puma, D.I. Kondarides, P. Lianos, Environ. Sci. Technol. 44 (2010) 7200–7205.
[33] V. Subramanian, E.E. Wolf, P.V. Kamat, J. Am. Chem. Soc. 126 (2004) 4943–4950.
[34] K. Dai, H. Chen, T.Y. Peng, D.N. Ke, H.B. Yi, Chemosphere 69 (2007) 1361–1367.
[35] L. Cao, Z. Gao, S.L. Suib, T.N. Obee, S.O. Hay, J.D. Freihaut, J. Catal. 196 (2000) 253–261.
[36] J. Yuan, H. Hu, M.X. Chen, J.W. Shiand, W.F. Shangguan, Catal. Today 139 (2008).
[37] M. Bencina, M. Valant, M.W. Pitcher, M. Fanetti, Nanoscale 16 (2014) 745–748.
[38] C. Wang, Z. Chen, H. Jin, C. Cao, J. Li, Z. Mi, J. Mater. Chem. A 2 (2014) 17820–17827.
[39] T. Tong, J. Zhang, T.F.B. Chen, D. He, J. Hazard. Mater. 155 (2008) 572–579.
[40] T. Umebayashi, T. Yamaki, H. Itoh, K. Asai, J. Phys. Chem. Solids 63 (2002) 1909–1920.
[41] Z. Li, W. Shen, W. He, X. Zu, J. Hazard. Mater. 155 (2008) 590–594.
[42] J. Zhu, W. Zheng, B. He, J. Zhang, M. Anpo, J. Mol. Catal. A – Chem. 216 (2004) 35–43.
[43] Z. Xu, I. Tabata, K. Hirogaki, K. Hisada, T. Wang, S. Wang, T. Hori, Mater. Lett. 65 (2011) 1252–1256.
[44] H. Widiyandari, A. Purwanto, R. Balgis, T. Ogi, K. Okuyama, Chem. Eng. J. 180 (2012) 323–329.
[45] A. Purwanto, H. Widiyandari, T. Ogi, K. Okuyama, Chem. Commun. 12 (2011) 525–529.
[46] Y. Sohn, Y. Smith, M. Misra, V. Subramanian, Appl. Catal. B-Environ. 84 (2008) 372–378.
[47] A.J. Bard, L.R. Faulkner, Electrochemical Methods, 2nd ed, John Wiley and Sons, New Jersey, 1980.
[48] A.J. Bard, J. Photochem. 10 (1979) 59–75.
[49] M. Wang, J. Ioccozia, L. Sun, C. Lin, Z. Lin, Energy Envrion. Sci. 7 (2014) 2182–2202.
[50] S. Tonda, S. Kumar, S. Kandula, V. Shanker, J. Mater. Chem. A 2 (2014) 6772–6780.
[51] S.H. Zhou, A.K. Ray, Ind. Eng. Chem. Res. 42 (2003) 6020–6033.
[52] F. Kiriakidou, D.I. Kondarides, X.E. Verykios, Catal. Today 54 (1999) 119–130.
[53] D. Bahnemann, Sol. Energy 77 (2004) 445–459.
[54] R. Comparelli, E. Fanizza, M.L. Curri, P.D. Cozzoli, G. Mascolo, R. Passino, A. Agostiano, Appl. Catal. B-Environ. 55 (2005) 81–91.
[55] G. Liu, C. Sun, H.G. Yang, S.C. Smith, L. Wang, G.Q. Lu, H.M. Cheng, Chem. Commun. 46 (2010) 755–757.
[56] G. Liu, L.S. Cheng, Y. Jin, H. Lu, L. Wang, S.C. Smith, G.Q. Lu, H.M. Cheng, J. Phys. Chem. C 113 (2009) 12317–12324.
[57] Y.J. Zhang, L.C. Liu, L.L. Ni, B.L. Wang, Appl. Catal. B: Environ. 138–139 (2013) 9–16.
[58] X. Yu, S. Liu, J. Yu, Appl. Catal. B: Environ. (2011) 12–20.